

From: "An anthology of developments in clinical engineering and bioimpedance: Festschrift for Sverre Grimnes", edited by Ø. Martinsen and Ø. Jensen, Unipub forlag, Oslo, Norway, 2009

Neurophysics: what the telegrapher's equation has taught us about the brain

Klas H. Pettersen and Gaute T. Einevoll

Department of Mathematical Sciences and Technology,
Norwegian University of Life Sciences, 1432 Ås
klas.pettersen@umb.no, gaute.einevoll@umb.no

1 Introduction

Neurons, the shrunken cells responsible for our mental capabilities, are utterly complex and non-linear in their signal processing. Both their morphologies and their behavior are highly entangled; each neuron typically receives signals from between 1000 and 10000 neurons impinging on its *dendrites*, the input branches of the neuron. These input signals are processed in the main cell body, the *soma*, of the neuron in such a way that the neuron either stays silent or fire an *action potential*. An action potential is an abrupt change in the neuron's *membrane potential*, i.e., the difference in potential between the inside and outside of the cell membrane, lasting a few milliseconds. When initiated in the soma, the action potential will propagate down the neuron's *axon*, the neuron's output channel, and convey information through *synapses* to other neurons. For a schematic overview of the basic constituent of a neuron, see Fig. 1. The generation of action potentials is a 'binary' all-or-nothing process: either a single action potential with a standardized shape is produced and propagated down the axon, or nothing happens at all.

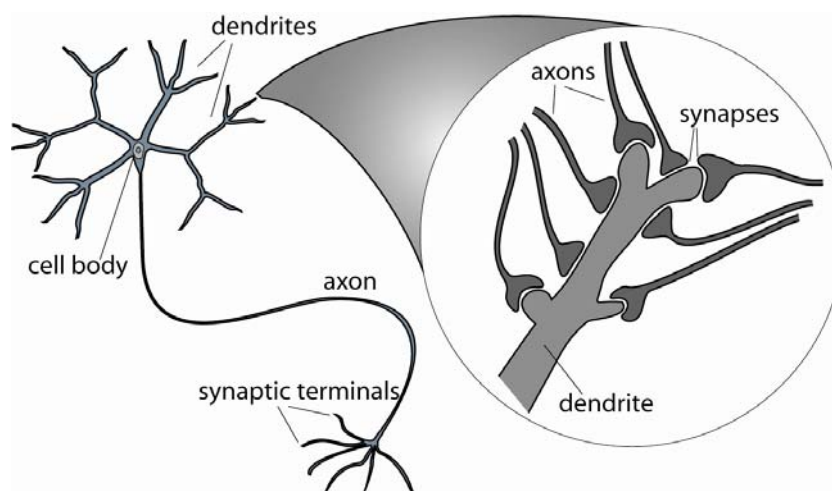


Figure 1: Schematic illustration of a neuron (nerve cell) and its synaptic connections.

One of the most prized achievements in theoretical biology is the establishment over the last hundred years or so of a mathematical theory for the signal processing in individual neurons. The most spectacular event is maybe the Nobel-prize winning work of Alan Hodgkin and Andrew Huxley in the early 1950s where they described the propagation of action potentials along the squid giant axon by a modified electrical circuit where the charge carriers are sodium, potassium, calcium, chloride and other ions flowing through and along the neuronal cell membrane [1-4]. This mathematical formulation could not only account for the results from tailored experiments used to construct the model and fit the model parameters; from their model they could also predict the shape and velocity of the action potential while moving down the axon. They calculated the propagation velocity of the action potential in their experimental system to be 18.8 meters per second which was roughly 10% off the experimental value of 21.2 meters per second [3]. Such quantitatively accurate model predictions are rare in theoretical biology.

Due to its stunning success in describing action potentials, the Hodgkin-Huxley approach was later generalized to include modeling of the signal processing properties of entire neurons, so called *compartmental modeling* [5-7], and also modeling of electrically excitable cells in the heart [8]. With the advent of compartmental modeling of neurons, computational neuroscientists now have a relatively firm starting point for mathematical explorations of neural activity. Thus neuroscience is presently among the biological sub-disciplines where the use of mathematical techniques is most established and recognized.

At the core of Hodgkin-Huxley theory and compartmental modeling of neurons lies the so called *cable equation* describing how the membrane potential dynamically spreads along a dendritic branch or an axon. This equation has a long and honorable history which can be traced back to the 'telegrapher's equation' explored by the (later) Lord Kelvin as early as 1855.

In this chapter we will briefly outline the origin of recordings of biological electrical activity and, in particular, the origin of the cable equation as used in computational neuroscience. The role of the cable equation in determining the signal processing in neurons, i.e., how input signals are converted into trains of action potentials, has received lots of attention [2-6]. Here we will instead focus on recent work from our group on how the cable equation determines the extracellular potentials recorded around neurons [9, 10].

2 History of electrical recordings in biology

For several centuries it has been known that mechanisms within the body both react to and create electricity. Already in 1786 the Italian Luigi Galvani began investigating the action of electricity upon the muscles of frogs [11]. This was the start of the research on what he called *animal electricity*, but it took a century before Augustus Waller in London was able to record the first human electrocardiogram (ECG) in 1887 [12]. One reason why this took such a long time was the lack of measuring devices with the desired sensitivity to measure the weak surface electricity of the body, in this case above the heart. Waller's ECG experiment was made possible by a breakthrough in techniques for measuring electrical potentials: around 1873 Gabriel Lippmann in Paris had invented the mercury capillary electrometer with a sufficient sensitivity. The capillary electrometer had a rather long adjustment time which resulted in a poor temporal

resolution, but in 1901 the dutch Willem Eintoven invented the string galvanometer [13]. This did not only have the required sensitivity, it also had an excellent temporal resolution. With his new measuring device Einthoven was able to measure and describe the human ECG in detail for which he received a Nobel prize in medicine in 1924.

As early as 1875 the englishman Richard Caton measured stimulus-evoked electric potentials at brain surfaces. He used a predecessor of the string galvanometer, a device known as a mirror galvanometer, and put electrodes directly onto the surfaces of the brains of rabbits. He observed that the recorded potentials varied when the retina was stimulated with different light intensities [14]. However, electrical recordings from the brain first became popular after the German Hans Berger in 1929 published his findings on measured electric fields originating from the human brain, recorded through the intact skull. Berger named his recordings 'electroencephalogram', which today are known as electroencephalograms (EEG).

3 Origin of cable equation

The first electrical brain recordings occurred at a time when it was still debated whether the neurons were physically connected in a joint meshwork or if they were separate computational entities. The latter view, called the *neuron doctrine*, was proven to be right. Actually, Fridtjof Nansen, the Norwegian explorer, scientist and diplomat, was one of the pioneers arguing for this doctrine. Nansen started his work in neuroscience in 1882, and in 1887 this resulted in the first Norwegian doctoral thesis in neurobiology titled '*The structure and combination of the histological elements of the central nervous system*'. Today the neuron doctrine is firmly established, and the neuron is generally accepted to be the basic computational unit in the brain.

The origin of the cable equation, the core ingredient of compartmental neuron models, is even older. In the early 1850s the question of a transatlantic telegraph line was raised, and the question appealed so much to the physicist William Thomson, later Lord Kelvin, that he started developing a mathematical theory for signal decay in underwater telegraph cables. In December 1856 when the Atlantic Telegraph Company was formed, Thomson was in fact also on its board of directors.

Thompson's mathematical model for the signal conduction through cables was based on Fourier's equations for heat conduction in a wire. This resulted in the so-called *telegraph* or *telegrapher's equation* describing the variation of voltage V along an electrical cable as function of time and position,

$$\frac{\partial^2 V}{\partial z^2} = LC \frac{\partial^2 V}{\partial t^2} + (LG + CR) \frac{\partial V}{\partial t} + RGV. \quad (1)$$

Here the resistance R and the inductance L represent series impedance along the cable, while the capacitance C and the leakage conductance G form the shunt admittance across the cable.

The inductive terms reflect so called *eddy currents*. Such currents are typically largest in thick, highly conductive cables, especially for high frequencies. Since neuronal cables have a relatively low inner (axial) conductivity and are very thin (certainly compared to the first transatlantic cable!), the inductive terms can safely be neglected for the typical frequencies

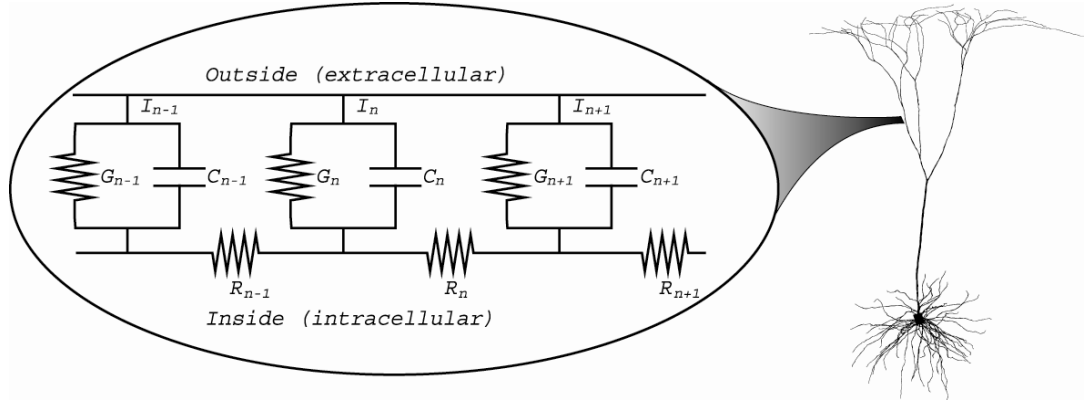


Figure 2: Illustration of equivalent-circuit modeling of a piece of neuronal cable by means of the *cable equation* in Eq. (2). For figure clarity a discretized version is illustrated, and the cable equation is obtained when the distance between neighboring circuit elements $n-1$ and n approaches zero [2-4]. The neuron depicted on the right is an anatomically reconstructed pyramidal neuron from cat visual cortex [15].

inherent in neuronal activity (<5000 Hz) . Therefore, for neuronal cables the inductive terms in Eq. (1) can be neglected, and the neuronal *cable equation* is thus given by

$$\frac{1}{R} \frac{\partial^2 V}{\partial z^2} = C \frac{\partial V}{\partial t} + GV. \quad (2)$$

Here the units of R , G , and C are ohms, siemens and fahrad per meter cable, respectively.¹ Fig. 2 illustrates the electrical circuit representation of a piece of neuronal cable from which the cable equation of Eq. (2) can be derived. For the idealized situation where the cable has a constant diameter, the electrical parameters R , G and C may be assumed to be constant. For realistic neurons, however, these electrical parameters will vary along the dendritic tree.

The cable equation is based on conservation of electrical current. The left hand side of Eq. (2) can be interpreted as the spatial gradient of the intracellular axial current. For charge to be conserved this change must correspond to the current that passes through the membrane, and the two terms on the right hand side correspond to the *capacitive* and *leak-resistance* transmembrane currents, respectively.

A more transparent version of the cable equation can be obtained by introducing the *length constant* λ given by

$$\lambda \equiv \sqrt{1/RG}, \quad (3)$$

and a *time constant* τ given by $\tau \equiv C/G$. Then the cable equation is given by

$$\lambda^2 \frac{\partial^2 V}{\partial z^2} = \tau \frac{\partial V}{\partial t} + V. \quad (4)$$

To explain generation and propagation of action potentials along the squid giant axon, Hodgkin and Huxley had to amend the cable equation with additional transmembrane currents through specialized *active* sodium and potassium ion channels [1]. These currents, described by complicated time- and voltage-dependent conductances, were essentially added to the right

¹For historical reasons we use the parameters G , R , and C throughout this chapter. In a neuroscience context the notation $r_m = 1/G$, $r_a = R$, and $c_m = C$ is more common [3].

hand side of the cable equation in Eq. (2). At the time the physical substrate of these currents was unknown, and phenomenological models extracted from experiments were used. Today it is known that these specialized ion channels correspond to various membrane-spanning proteins whose structure in turn is encoded in the DNA. So from a mathematical point of view one might say that evolution has fiddled around with the right hand side of the cable equation for millions of years to provide us with the basic element of thinking.

Wilfrid Rall, among the first proper computational neuroscientists [16], was a pioneer in the application of the cable equation to understand the signal processing properties of neurons, in particular how the dendrites integrate synaptic inputs. He was trained as a physicist during the second world war and worked on the Manhattan project. After the war he moved to University of Chicago to attend a biophysics program organized by Kenneth S. Cole, known for the Cole impedance and Cole-Cole permittivity equations [17], and others, and Rall soon became a leading figure in the mathematical neuroscience community. In a paper in 1959 he describes the historical development of the cable equation [18]:

The mathematical treatment of axonal electrotonus [alteration in excitability and conductivity of a nerve or muscle during the passage of an electric current through it] began in the 1870s with the work of Hermann (1872,1879) supported by Weber's (1873) mathematical analysis of the external field in the surrounding volume conductor. Hermann recognized the mathematical analogy of this problem with the analog in heat conduction, but the analogy with Kelvin's (1855) treatment of the submarine telegraph cable in the 1850s was first recognized by Hoorweg in 1898. This cable analogy was developed independently by Cremer (1899,1909) and by Hermann (1905) early in the 20th century and has been widely used since that time. These mathematical analogies are important because of the extensive literature devoted to both general mathematical methods and special solutions applicable to problems of this kind (Carslaw and Jaeger, 1939). Important papers on the steady-state distributions of axonal electrotonus are those of Rushton (1927, 1934) and Cole and Hodgkin (1939) published in the 1920s and 1930s. The two most useful mathematical presentations of axonal electrotonus (including consideration of transients) are those provided by Hodgkin and Rushton (1946) and Davis and Lorente de No (1947) in the 1940s.

In present-day compartmental modeling the neuronal cables are divided into compartments where each compartment essentially is modeled by a discretized version of the cable equation with various transmembrane currents accounting for the action of the various ion channels [4-7], see Fig. 2. Mathematically the neuron is expressed as a system of coupled differential equations, and free simulation tools such as NEURON [19] and Genesis [20] have been tailor-made to solve these equations efficiently.

4 Modeling of extracellular signatures of action potentials

Most of what we know about the functioning of neurons and neural networks has come from electrophysiological recordings, i.e., recordings of electrical potentials in the brain using electrodes. In *intracellular recordings* an extremely thin electrode is poked through the neuronal

membrane so that the membrane potential, i.e., the variable V in the cable equation, can be measured directly. Intracellular recordings are technically challenging, in particular in living animals, and the work-horse of brain electrophysiology *in vivo* has been *extracellular* recordings. In such recordings the potential in the extracellular medium is typically measured relative to a distant reference electrode. Extracellular potentials are much smaller than intracellular potentials; while a typical membrane potential is 60-80 millivolts, the extracellular potential is typically much less than a millivolt. The extracellular potentials stem from a weighted sum over all transmembrane currents in the vicinity of the electrode tip and are in general much harder to interpret than intracellularly recorded membrane potentials.

However, if the electrode is placed very close to the soma of a neuron firing action potentials, the recorded extracellular potential will largely be dominated by the strong and characteristic soma currents affiliated with the action potentials. Each action potential will then be recognized by a characteristic spiky voltage trace in the recorded extracellular potential. The counting of these extracellular spikes can be used to record the train of action potentials from this neuron. In general, however, spikes from many active neurons may be picked up by the electrode, and several issues arise when such recordings are interpreted, e.g., which types of cells are most likely to be seen in the recordings, which cell parameters are important for the spike amplitude and shape, and which parameters are important for the decay of the spike amplitude with increasing distance from the neuron? It turns out that the cable equation is essential for understanding how intracellular action potentials are 'translated' into extracellular spikes, and in this section we will outline results from a previous study by us where this question was investigated in detail [9].

4.1 Forward modeling scheme

Neuronal activity can be computed analytically from the cable equation only for the simplest neuron models. For more complicated neuron models, compartmental simulation tools like NEURON [19] or Genesis [20] must be used to calculate the transmembrane currents acting as sources for the extracellular potential. With all transmembrane currents and their spatial positions known, the extracellular potential at any point in the brain can in principle be computed using Maxwell's equations. However, this presupposes that the electrical properties of the surrounding medium are known. Mathematically, this can be done by numerically solving a variant of Poisson's equation [21] using finite-element methods (FEM). Here, however, a mathematically and conceptually simpler forward-modeling scheme will be used [9, 10, 22].

In our compartmental modeling scheme a neuron is divided into N compartments, and the transmembrane current from each compartment is denoted $I_n(t)$. One can then derive the following formula for the extracellular potential $\phi(\mathbf{r}, t)$ due to activity in this particular neuron [21, 22],

$$\phi(\mathbf{r}, t) = \frac{1}{4\pi\sigma} \sum_{n=1}^N \frac{I_n(t)}{|\mathbf{r} - \mathbf{r}_n|}, \quad (5)$$

where σ is the extracellular conductivity, and compartment n is positioned at \mathbf{r}_n . In deriving this formula, the following assumptions and approximations are used:

1. *Quasistatic approximation of Maxwell's equations.* This amounts to neglecting the terms with time derivatives of the electric field \mathbf{E} and magnetic field \mathbf{B} from the original Maxwell's equations so that the electromagnetic field effectively decouples into separate 'quasistatic' electric and magnetic fields [23]. Then the electric field \mathbf{E} in the extracellular medium is related to the extracellular potential ϕ via $\mathbf{E} = -\nabla\phi$. For frequencies inherent in neural activity, i.e., less than a few thousand hertz, the quasistatic approximation seems to be well fulfilled (see argument on p. 426 of [23]).
2. *Extracellular medium* is assumed to be
 - *linear*, i.e., $\mathbf{j} = \sigma\mathbf{E}$, where \mathbf{j} is the current density,
 - *ohmic*, i.e., no imaginary part of σ [24, 25],
 - *position-independent*, i.e., σ is the same everywhere [25], and
 - *isotropic*, i.e., same σ in all directions [25].

For a more comprehensive discussion of these assumptions regarding the extracellular medium, and also ways of generalizing Eq. (5) when the assumptions do not apply, see Ref. [26].

4.2 Effect of dendritic filtering on extracellular potential

In Fig. 3A we show a typical shape of an *intracellular* action potential calculated by the simulation tool NEURON using a model pyramidal neuron constructed and made publicly available by Mainen and Sejnowski [15]. This model has several types of active ion channels spread across the neuronal membrane. (For simulation details see Ref. [10].) The membrane voltage trace has a characteristic shape with a fast *depolarizing* phase (from about -55 mV to almost 20 mV in a fraction of a millisecond), followed by an almost equally fast *repolarization*, and then a longer *hyperpolarizing* phase (membrane potential more negative than the resting potential).

The corresponding extracellular spike patterns at different spatial positions are shown in Fig. 3B. These extracellular potentials are found from evaluating a sum of the type in Eq. (5) where $I_n(t)$ corresponds to the transmembrane currents found for each compartment in the NEURON simulation². Several features are notable:

- The extracellular spike has a much lower amplitude than the intracellular action potential. Even close to the soma the amplitude is less than a few tens of microvolts, more than a factor thousand smaller than the intracellular amplitude.
- Not only the size, but also the shape of the extracellular potential vary significantly with position. The shape around the apical (upper) dendrites is typically inverted compared to around the basal (lower) dendrites.
- The spike width increases with increasing distances from the soma. This is highlighted by the insets showing magnified extracellular signatures: the extracellular spike-width, defined as the width of the first rapid phase at 25% of its maximum amplitude, is seen to increase from 0.625 ms close to soma (bottom inset) to 0.75 ms further away (top inset).

²Eq. (5) corresponds to a *point-source* approximation where the total transmembrane current from each compartment is assumed to come out from a single point. In the evaluation of Fig. 3B we have instead used the *line-source* approximation where the transmembrane current is assumed to be evenly spread along a line, see [9].

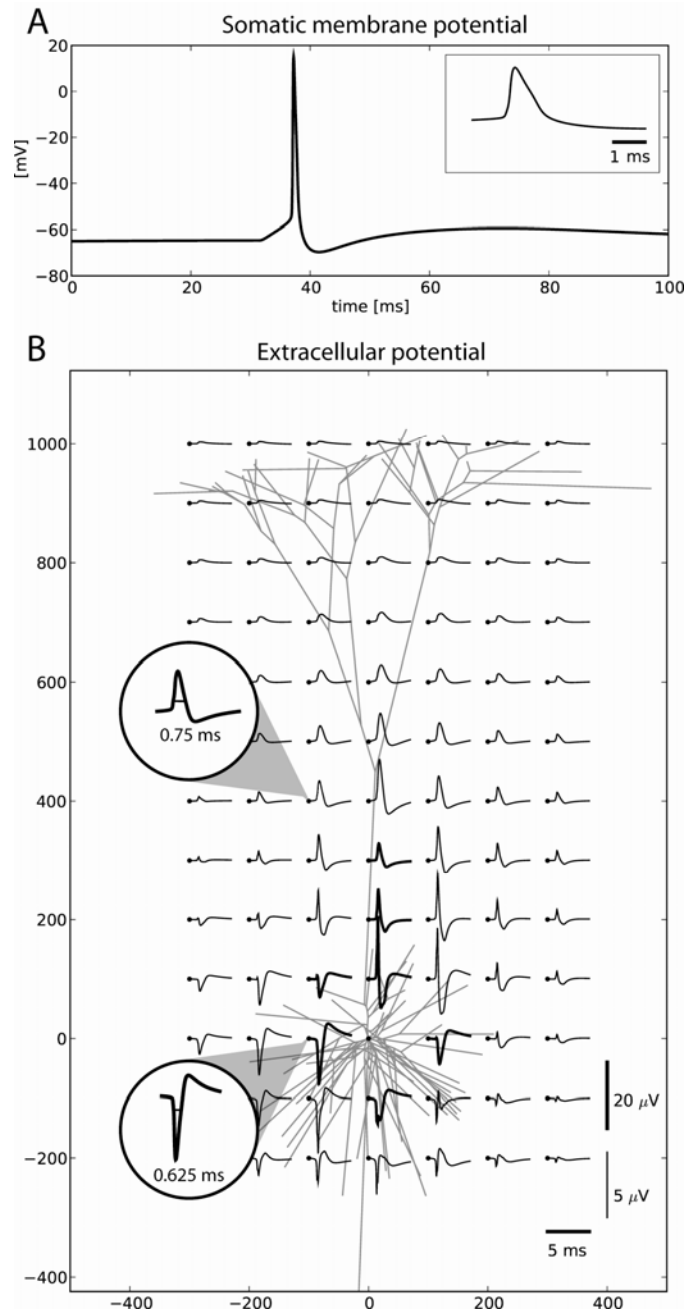
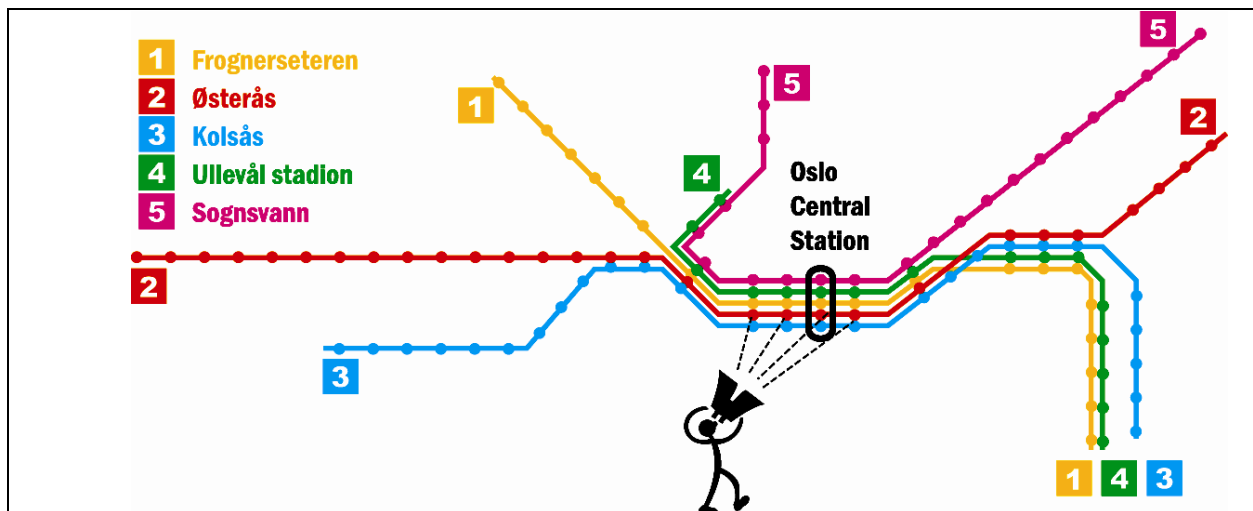


Figure 3: Intracellularly and extracellularly recorded action potentials. The model is a reconstructed pyramidal neuron taken from Ref. [15]. A synaptic stimuli similar to what is called 'synaptic input pattern 1' in Ref. [10] is used. (A) Soma membrane potential during an action potential. Inset shows the membrane potential trace in a five-millisecond time window around the action potential. (B) Calculated extracellular potentials based on a variant of the forward-modeling formula in Eq. (5) (i.e., the line-source approximation, see [10]) assuming an isotropic, homogenous and purely conductive extracellular medium with $\sigma=0.3$ S/m. The extracellular potentials are shown for the same five milliseconds as in the membrane potential inset in (A). All distances are in micrometers. Note that the potentials in the insets are not to scale.



Extracellular vs. intracellular potentials. Intracellular and extracellular potentials are often confused, and modelers sometimes compare their model predictions of *intracellular* potentials (which are easier to model) with recorded *extracellular* potentials (which are easier to measure). As seen in Fig. 3 the connection between intracellular and extracellular is not trivial, however. To illustrate this further we consider the above map of the Oslo subway system. With its branchy structure of different lines ('dendrites') stretching out from the hub at Oslo Central Station ('soma'), the subway system resembles a neuron. If we pursue this analogy, the subway stations (marked with dots) may correspond to 'neuronal compartments' and the net number of passengers entering or leaving the subway system at each station to the net 'transmembrane current' at this 'compartment'. If more passengers enter than leave the subway system at a point in time, it means that the number of people in the subway system, i.e., the 'intracellular membrane potential', increases. (If we introduce a 'capacitive current' corresponding to the *change* in the number of people inside each station, we can even get a 'current conservation law'.) The intracellular soma membrane potential, crucial for predicting the generation of neuronal action potentials (which luckily has no clear analogy in normal subway traffic), would then correspond to the number of passengers within the subway station at Oslo Central Station. The extracellular potential on the other hand would be more similar to what could be measured by an eccentric (at best) observer counting passengers flowing in and out of a few neighboring subway stations (with binoculars on the top of a large building maybe). While the analogy is not 100%, it should illustrate that while intracellular and extracellular potentials are correlated quantities, they are really two different things.

The spike-width increase implies that the higher frequencies contained in the action potential attenuate more steeply than the lower frequencies as a function of distance from the soma. Such a spike-width increase has been seen experimentally, and one proposed explanation for the effect is that the extracellular medium acts as a low-pass filter, for example through frequency-dependent polarization of cell membranes [27, 28]. However, direct measurements of the impedance spectrum for cortical tissue for the relevant frequencies have given conflicting results: while Gabriel and coworkers [29] claimed to find such frequency-dependent filtering, Logothetis and colleagues [25] measured no such filtering.

In Fig. 3B we see that distance-dependent low-pass frequency filtering of the extracellular spikes (i.e., change in spike width) is seen also for our homogenous, isotropic and purely conductive medium with no inherent frequency filtering. In accordance with this we thus proposed in Ref. [9] that the neuron *morphology*, combined with its *cable properties* gives an

alternative explanation for the observed increase in low-pass filtering with increasing distance from the soma.

4.3 Physical origin of dendritic filtering

Numerical exploration of a variety of neuron models in Ref. [9] showed that the distance-dependent low-pass filtering effect for the extracellular potential is a generic property of neurons. The physical origin lies in the cable equation itself, and the neuronal *length constant* briefly introduced in Eqs. (3-4) turns out to be a key concept.

Let us first consider the simple *infinite ball-and-stick* neuron model consisting of a spherical soma connected to an infinitely long dendritic stick of constant diameter d described by the cable equation [2, 9], see Fig. 4. This ball-and-stick neuron is further assumed to have an inward steady-state (DC) transmembrane current in the soma. Since the transmembrane currents at all times have to sum to zero, the same amount of current has to leave through the dendritic stick. From the solution of the cable equation it follows that the density function of the dendritic return current decays exponentially with distance from the soma with the length constant $\lambda = \sqrt{1/RG}$ [2, 9]. It is customary to describe λ in *specific* parameters, i.e., parameters that only depend on the physical properties of the membrane and the intracellular medium. Then we have $\lambda = \sqrt{dR_m/4R_i}$ where R_m is the membrane resistivity [Ωcm^2], and R_i is the axial resistivity [Ωcm] [3, 9]. In the DC situation the length constant λ also corresponds to the dendritic position where the steady-state return current has decreased to $1/e$ of its value at the soma, or alternatively, the position where the dendritic return current has its *center of gravity*. The center of gravity is then defined as the mean of the normalized transmembrane current density weighted by dendritic position [9].

The length constant is not only an important measure when describing the neuron's intrinsic qualities (for example electrotonic compactness, i.e., how much the membrane potential varies across the neurons) [2, 3]. It is also very useful for understanding the neuron's extracellular potential. For example, when computing the extracellular potential far away from an active neuron firing an action potential, the ball-and-stick neuron may be approximated by an even simpler model, the *dipole model* [9]. Then all the return current is assumed to cross the dendritic membrane through a single point a distance λ above the soma, so that the system effectively is described as a (transmembrane) current dipole of length λ , cf. Fig. 4.

Traditionally the length constant is only defined for the DC situation, and only for infinite cables. We here define a more general alternating-current (AC) length constant $\lambda_{AC}(\omega)$ applicable also for dendritic sticks of finite length. The DC length constant can be considered to be the weighted mean position of the DC return current, and in analogy to this we define the generalized, frequency-dependent length constant to be

$$\lambda_{AC}(\omega) = \frac{\int_0^l z |\hat{i}_m(z)| dz}{\int_0^l |\hat{i}_m(z)| dz}, \quad (6)$$

where $\omega = 2\pi f$ is the angular frequency, and $|\hat{i}_m(z)|$ is the amplitude of the sinusoidally oscillating transmembrane current at a position z when a sinusoidal current is injected in the

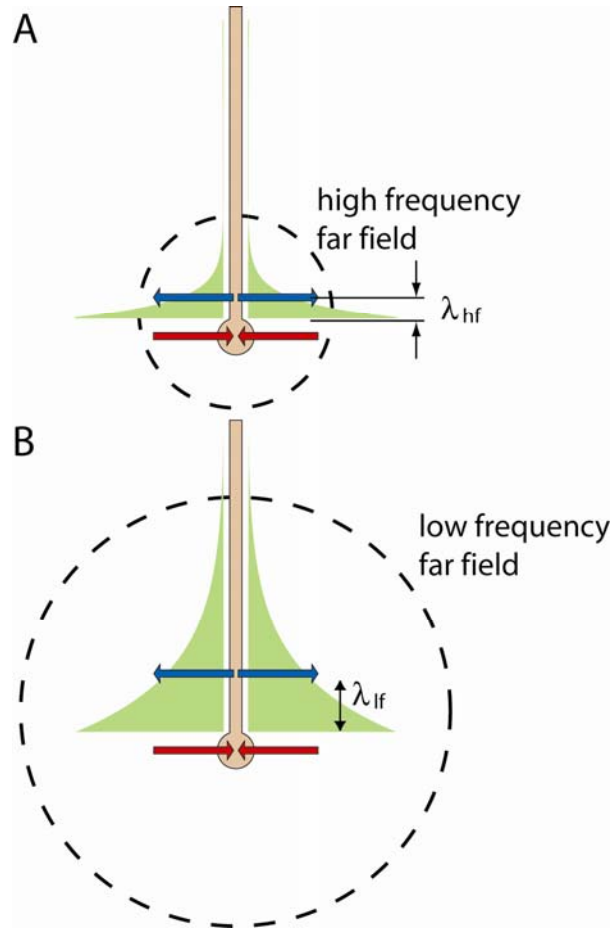


Figure 4: Illustration of ball-and-stick neuron and its transmembrane return current density following current injection in the soma (lower arrows). The dipole size (distance between upper and lower arrows) is illustrated both for a high (λ_{hf}) and a low (λ_{lf}) frequency (B). The dashed circles illustrate the distance at which the transition to the far-field limit occurs.

soma [9]. The dendritic stick is assumed to be oriented along the positive z -axis from $z = 0$ (soma position) to $z = l$. For an infinite stick Eq. (6) reduces to [2, 9]

$$\lambda_{AC}^{\infty}(\omega) = \lambda \sqrt{2/[1 + \sqrt{1 + (\omega\tau)^2}]}, \quad (7)$$

with τ denoting the membrane time constant, $\tau = C/G = R_m C_m$ where C_m is the specific membrane capacitance.

The main feature of the functional dependence of $\lambda_{AC}(\omega)$ is that it decreases with increasing frequency, cf. Fig. 4B in Ref. [9]. The intracellular action-potential waveform, cf. Fig. 3A, consists of a combination of frequency components, and each component can be viewed as a somatic voltage source forcing sinusoidally varying currents into the dendritic stick. The decrease of $\lambda_{AC}(\omega)$ with frequency implies that the return currents on average will be located closer to the soma for the highest frequency components than for the lowest frequency components, and thus make smaller current dipole lengths.

With the dendritic stick described by the *linear* cable equation, each frequency component of the action potential can be considered independently. Further, if the dipole model is considered for the ball-and-stick neuron, we expect that each frequency component shows a $1/r$ decay with distance close to the soma, while a much sharper $1/r^2$ decay is expected in the far-field limit [9]. The key point regarding low-pass filtering is that the *transition* to the far-field limit will depend on the current dipole length, i.e., the AC length constant $\lambda_{AC}(\omega)$, and thus implicitly on the frequency. The higher frequency components will thus reach their far-field limits, where they are strongly attenuated, closer to the soma than the low-frequency components, see Fig. 4. The net effect will be a low-pass filtering, i.e., an increase in the spike width with distance from soma [9]. Note that this reasoning applies also to neurons with more complicated geometries, e.g., with numerous dendritic sticks protruding from the somas, since the contributions to the extracellular potential add up linearly. This generic low-pass filtering effect was in fact confirmed by direct numerical calculations for several different neuronal morphologies in Ref. [9].

4.4 What determines the neuron's horizon of visibility?

Our dipole approximation to the ball-and-stick model can also give important insights into how the neuronal morphology and membrane parameters affect the *size* (peak-to-peak amplitude) of the extracellular spike [9]. By considering each frequency component of the action potential individually one can derive a frequency-dependent *transfer function* T mapping the intracellular somatic membrane potential to the extracellular potential. This transfer function reveals how the extracellular spike amplitude will depend on the dendritic parameters (given a particular intracellular action potential). The derivation is somewhat involved, see Ref.[9], but the final expressions near the soma and in the far-field limit are

$$|T_{\text{near}}| \sim \frac{1}{\sigma} d^{3/2} \sqrt{\frac{fC_m}{R_i}} \frac{1}{r}, \quad |T_{\text{far}}| \sim \frac{1}{\sigma} \frac{d^2}{R_i} \frac{1}{r^2}, \quad (8)$$

respectively³.

A notable feature of these expressions is the *absence* of the membrane resistance R_m ; thus, the size and shape of the extracellular spike is predicted to be independent of this quantity. We further see that the transfer function, and thus the size of the extracellular spike, will decrease with increasing axial resistance R_i inside the dendrite. However, the dominating intrinsic neuronal parameter appears to be the dendritic stick diameter d . We see that the transfer function is predicted to grow as $d^{3/2}$ near the soma and as d^2 further away. This result also applies to situations where one has several dendritic sticks attached to the soma [9]. A rough rule of thumb deduced from these considerations is that *a neuron's extracellular spike amplitude is approximately proportional to the sum of the dendritic cross-sectional areas of all dendritic branches connected to the soma*. Thus, neurons with many, thick dendrites connected to soma will produce large-amplitude spikes, and will therefore have the largest radius of

³This 'far-field' expression for the ball-and-stick neuron transfer function is not valid when moving horizontally away from the soma. In this direction the transfer function is given by a far-field quadrupolar expression, see. Eq. (24) in Ref. [9].

visibility. The validity of this rule of thumb was shown by direct numerical simulations in Ref. [9], also for morphologically reconstructed neurons with complicated dendritic geometries.

5 Concluding remarks

The modest-looking cable equation now has a more than 150 year long history, but will not retire soon. The birth of the equation was certainly spectacular describing signal processing in the transatlantic telegraph cable, the most challenging and prestigious technological project of its time. But the future is maybe even brighter. One of the most exciting research projects of this century is to figure out how we think. It is difficult to know for sure whether mankind eventually will be able to sort this out, but if we do, the cable equation will have to be at center stage.

Acknowledgment: We thank Henrik Lindén for help with making Figure 3.

References

- [1] Hodgkin AL, Huxley AF. A quantitative description of membrane current and its application to conduction and excitation in nerve. *J Physiol.* 1952; 117:500-544.
- [2] Johnston D, Wu SMS. *Foundations of Cellular Neurophysiology.* Cambridge, MA: MIT Press; 1994.
- [3] Koch C. *Biophysics of Computation.* New York: Oxford University Press; 1999.
- [4] Dayan P, Abbott LF. *Theoretical Neuroscience.* Cambridge, MA: MIT Press; 2001.
- [5] Koch C, Segev I (eds). *Methods in Neuronal Modeling (2nd ed).* Cambridge, MA: MIT Press; 1998.
- [6] Bower JM, Beeman D (eds). *The Book of Genesis: Exploring Realistic Neural Models with the General Neural Simulation System (2nd ed).* New York: Springer, 1998.
- [7] De Schutter E (ed). *Computational Neuroscience: Realistic Modeling for Experimentalists.* Boca Raton: CRC Press; 2000.
- [8] Noble D. *The Initiation of the Heartbeat.* Oxford: Clarendon Press; 1979.
- [9] Pettersen KH, Einevoll GT. Amplitude variability and extracellular low-pass filtering of neuronal spikes. *Biophys J.* 2008; 94:784-802.
- [10] Pettersen KH, Hagen E, Einevoll GT. Estimation of population firing rates and current source densities from laminar electrode recordings. *J Comput Neurosci.* 2008; 24:291-313.
- [11] Galvani L. *De viribus electricitatis in motu musculari : Commentarius.* Bologna : Tip. Istituto delle Scienze. 1791; 58.
- [12] Waller AD. A Demonstration on Man of Electromotive Changes accompanying the Heart's Beat. *J Physiol.* 1887; 8:229-234.
- [13] Einthoven W. Un nouveau galvanometre. *Arch Neerl Sc Ex Nat.* 1901; 6:625-633.
- [14] Finger S. *Origins of Neuroscience: a history of explorations in brain function.* New York: Oxford University Press; 1994.
- [15] Mainen ZF, Sejnowski TJ. Influence of dendritic structure on firing pattern in model neocortical neurons. *Nature.* 1996; 382:363-366.
- [16] Segev I (ed). *The Theoretical Foundation of Dendritic Function: Selected Papers of Wilfrid Rall with Commentaries.* Cambridge, MA: MIT Press; 1995.
- [17] Grimnes S, Martinsen G. *Bioimpedance and Bioelectricity basics, 2nd ed.* New York: Academic Press; 2008.
- [18] Rall W. Dendritic current distribution and whole neuron properties. *Naval Medical Research*

Institute Research Report. 1959; NM 0105 00.01.02:479-525.

[19] Carnevale NT, Hines ML. The NEURON Book. Cambridge University Press; 2006. Available from: <http://neuron.duke.edu>.

[20] Bower JM, Beeman D. The Book of GENESIS: Exploring Realistic Neural Models with the GEneral NEural Simulation System, Second edition. Springer-Verlag, New York; 1998. Available from: <http://www.genesis-sim.org>.

[21] Nicholson C, Freeman JA. Theory of current source-density analysis and determination of conductivity tensor for anuran cerebellum. *J Neurophysiol.* 1975; 38:356-368.

[22] Holt GR, Koch C. Electrical interactions via the extracellular potential near cell bodies. *J Comput Neurosci.* 1999; 6:169-184.

[23] Hamalainen M, Hari R, Ilmoniemi RJ, Knuutila J, Lounasmaa OV. Magnetoencephalography theory, instrumentation, and applications to noninvasive studies of the working human brain. *Rev Mod Phys.* 1993; 65:413-497.

[24] Nunez PL. *Electric Fields of the Brain: The Neurophysics of EEG.* Oxford University Press ; 2006.

[25] Logothetis NK, Kayser C, Oeltermann A. In vivo measurement of cortical impedance spectrum in monkeys: implications for signal propagation. *Neuron.* 2007; 55:809-823.

[26] Pettersen KH, Linden H, Dale AM, Einevoll GT. Extracellular spikes and multi-electrode recordings. To appear in *Handbook of Neural Activity Measurement*, eds: Brette R, Destexhe A. Cambridge, UK: Cambridge University Press.

[27] Bedard C, Kroger H, Destexhe A. Modeling extracellular field potentials and the frequency-filtering properties of extracellular space. *Biophys J.* 2004; 86:1829-1842.

[28] Bedard C, Kroger H, Destexhe A. Model of low-pass filtering of local field potentials in brain tissue. *Phys Rev E.* 2006; 73:051911.

[29] Gabriel S, Lau RW, Gabriel C. The dielectric properties of biological tissues: II. Measurements in the frequency range 10 Hz to 20 GHz. *Phys Med Biol.* 1996; 41:2251-2269.